Available online at www.sciencedirect.com
SCIENCE DIRECT®
Journal of the European Ceramic Society 24 (2004) 3635–3641
www.elsevier.com/locate/jeurceramsoc

Microstructure and electrical characteristics of $ZnO–B_2O_3–PbO–V_2O_5–MnO_2$ ceramics prepared from ZnO nanopowders

Jun Wu, Changsheng Xie*, Junhui Hu, Dawen Zeng, Aihua Wang

The State Key Laboratory of Plastic Forming Simulation and Mould Technology, Department of Materials Science and Engineering, Huazhong University of Science and Technology, Wuhan 430074, PR China

Received 6 August 2003; received in revised form 13 December 2003; accepted 27 December 2003

Available online 17 April 2004

Abstract

A peculiar kind of $ZnO–B_2O_3–PbO–V_2O_5–MnO_2$ ceramics was produced from the ZnO nanopowders directly co-doped with the oxides instead of lead zinc borate frit in this investigation. The 8 wt.% ($PbO + B_2O_3$) co-doped ceramics sintered at 950 °C for 2 h displayed the optimum electrical properties, that is, leakage current density $J_L = 6.2 \times 10^{-6}$ A/cm^2, nonlinear coefficient $\alpha = 22.8$ and breakdown voltage $V_{BK} = 331$ V/mm. The co-doping of 8 wt.% ($PbO + B_2O_3$) resulted in an increase in nonlinear coefficient and a decrease in leakage current density of the $ZnO–V_2O_5$ varistors while the sintering temperature showed no evident influence on nonlinear coefficient and leakage current density at the range of 800–950 °C.

Keywords: ZnO; Varistors; Electrical properties; Grain boundaries; Sintering

1. Introduction

ZnO semi-conductive ceramics with several oxide additives, such as Bi, Sb, Co, Cr, Mn oxides, have been widely used as voltage regulators and surge current protectors because of their high nonlinear voltage–current characteristics.[1–6] It is believed that these characteristics arise from the modifications of the zinc oxide grain boundaries caused by the segregation of some special dopant such as Bi,[7] Pr[8,9] and Ba.[10] Recently, it is reported that V_2O_5[11–14] and lead zinc borosilicate glass[15–20] are varistor-forming ingredient for ZnO ceramics, the use of these materials results in varistor properties that is similar to those of $ZnO–Bi_2O_3$ system. The advantages of $ZnO–V_2O_5$ system are that the ceramics can be sintered at a relatively low temperature (such as 900 °C)[21] in a conventional electric furnace, and the addition of V_2O_5 markedly enhances the densification rate and grain growth[22,23] simultaneously. This is important for multilayer varistors because such ceramics can be co-sintered with a relatively cheaper inner electrode, such as silver electrode, which has a melting point of about 960 °C.[14] It is also found that the liquid-phase sintering of lead zinc borosilicate glass at low temperature is similar to that of Bi_2O_3 whose melting point is 880 °C, and the influence of borosilicate glass on electrical properties is also similar to that of Bi_2O_3.[15,16]

It is worthy to notice that the maximum nonlinear coefficient of binary $ZnO–V_2O_5$ system with 0.25 mol% V_2O_5 doped is only 8.9 when sintered at 900 °C for 4 h,[13] and the maximum nonlinear coefficient of 22–23.5 and the minimum leakage current density of 1.4×10^{-6} to 2.4×10^{-6} A/cm^2 are acquired when 0.5 mol% V_2O_5 and 0.3 mol% Mn_3O_4 co-doped ceramics are sintered at 900 °C for 30 min or 1100 °C for 10 min in a microwave furnace.[22,23] There are also some reports on the effects of other additives, such as Mn_3O_4, CoO, NiO, Nb_2O_3, Na-glass,[14] MnO_2 and Sb_2O_3,[24,25] on microstructure and electrical properties. Among these additives, MnO_2 displays the most significant influence on varistor performance, and the corresponding optimum content is 1 mol% MnO_2 and 0.5 mol% V_2O_5.[24] Even though the melting point of V_2O_5 is about 690 °C, the sintering temperature of $ZnO–V_2O_5$ ceramics will rapidly

* Corresponding author. Tel.: +86-27-87543840.
E-mail address: csxie@mail.hust.edu.cn (C. Xie).

0955-2219/$ – see front matter © 2004 Elsevier Ltd. All rights reserved.
doi:10.1016/j.jeurceramsoc.2003.12.013

rise when several additives are co-doped. For example, it is not fully densified when sintered at 900 °C and a higher temperature of 1200 °C has to be used for $ZnO–V_2O_5–Sb_2O_3$ ceramics.[24,25]

On the other hand, the amorphous lead zinc borosilicate frit should be prepared in advance as raw materials in the previous work.[16,20] This method is relatively complicated and it is difficult to ensure the accuracy and repetition of the component of frit, which plays a very important role in electrical properties of varistors.

It should be indicated that ZnO nanopowders have high activity so as markedly to decrease sintering temperature. Furthermore, ZnO powders could exist in many kinds of shapes, in which normally one is spheroid and the other is tetrapod.[26–28] Some researchers prepared ZnO varistors from nanometer powders by sol–gel,[29] chemical co-precipitation and plasma pyrolysis,[30] but it still belongs to $ZnO–Bi_2O_3$ system and the powders are still spheroid. The sol–gel glass-coated zinc oxide is also applied for varistor,[31] however, its nonlinear coefficient is too small to be applied in practice. The nanosized doped-ZnO ceramic powders prepared by metallorganic polymeric method could markedly decrease sintering temperature, and the normal liquid-phase sintering occurred at 850 °C,[32] but the breakdown voltage V_{BK} is too high (≥1500 V/mm).

In the previous work,[33] ZnO-glass varistors are prepared from the tetrapod ZnO nanopowders with a kind of noble method, namely, direct co-sintering of the glass forming oxides with other starting materials for the varistors preparation. In present work, the $ZnO–B_2O_3–PbO–V_2O_5–MnO_2$ varistors are prepared from the same type of ZnO nanopowders and with the same method mentioned in the previous work,[33] the microstructures and the electrical properties of this noble system are also investigated.

2. Experimental procedure

The raw ZnO nanopowders prepared by a vaporization condensation technique were used as matrix material, and V_2O_5, MnO_2, PbO, and B_2O_3 with reagent grade were used as additives, in which the ratio of PbO to B_2O_3 was kept constant. The mixtures of above materials with different proportions were ball-milled for 8 h and then pressed into discs of 20 mm in diameter at a pressure of about 200 MPa while 2% ethyl cellulose was added as binder, finally the green discs with a relative density of about 60%TD (TD = 5.645 g/cm^3) were obtained. The as-prepared discs were sintered at a temperature range from 500 to 950 °C in air for 2 and 4 h in a conventional electric furnace and then furnace cooled to room temperature. A silver paste was printed on both sides of the sintered discs (about 15 mm in diameter), and then the silver-printed discs were sintered at 500 °C in air for 15 min with an aim to prepare samples for electrical characteristic experiments. The electrical characteristic test parameters were as follows: the voltage at a current of 1 mA (i.e. the breakdown voltage, V_{BK}), the current density at a voltage of 0.83 V_{BK} (i.e. leakage current density, J_L), and the nonlinear coefficient α which can be estimated by the following equation:

$$\alpha = \frac{1}{\log(V_{1\,mA}/V_{0.1\,mA})} \quad (1)$$

where $V_{1\,mA}$ and $V_{0.1\,mA}$ represent the voltages at 1 and 0.1 mA, respectively.

The voltage–current (*V–I*) characteristics of the sintered ceramics were measured by a variable DC power source.

The surface microstructures of the samples were examined by HITACHI S-570 scanning electron microscope. The crystalline phases of the samples were identified by D/max-IIIC X-ray diffraction (XRD) with Cu target (λ = 0.15406 nm).

The radial shrinkage ratio of the samples, one of the methods to represent the relative density of the sintered ceramics, was determined by the following equation:

$$\frac{\Delta l}{l_0} = \frac{l_0 - l_s}{l_0} \quad (2)$$

where l_0 and l_s represent the diameters of the green and sintered ceramics, respectively.

3. Results and discussion

Fig. 1 shows XRD patterns of the sintered ceramics. It is evident that the main phase of all the samples is ZnO, which is exactly the same as the JCPDS card (No. 36-1451), but the second phase is relatively difficult to identify exactly since its peak strength is too weak. Table 1 summaries the d-spacing data of the samples measured by XRD and of γ-$Zn_3(VO_4)_2$ (JCPDS card No. 19-1470), β-$Pb_3(VO_4)_2$ (JCPDS card No. 31-0698) and ZnO (JCPDS card No. 36-1451) quoted from the JCPDS cards. The phase β-$Pb_3(VO_4)_2$ is hard to be distinguished from the XRD patterns because the main peaks of β-$Pb_3(VO_4)_2$ are nearly

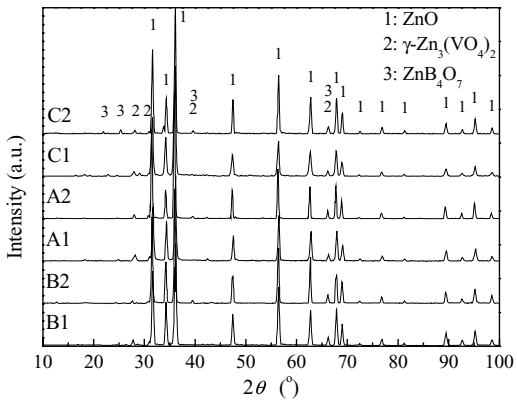

Fig. 1. XRD patterns of the samples, A1, A2: 8 wt.% ($PbO + B_2O_3$); B1, B2: 4 wt.% ($PbO + B_2O_3$); C1, C2: 12 wt.% ($PbO + B_2O_3$). A1, B1, C1: sintered at 800 °C for 2 h; A2, B2, C2: sintered at 900 °C for 2 h.

Table 1
Summary of d-spacing data of the samples, γ-$Zn_3(VO_4)_2$, γ-$Pb_3(VO_4)_2$ and ZnO

d-spacing data of the samples measured by XRD, *d* (Å)	γ-$Zn_3(VO_4)_2$ (JCPDS card No. 19-1470)		β-$Pb_3(VO_4)_2$ (JCPDS card No. 31-0698)		ZnO (JCPDS card No. 36-1451)	
	d (Å)	I/I_0	*d* (Å)	I/I_0	*d* (Å)	I/I_0
3.206–3.164	3.1800	85	3.1990	100	–	–
–	3.1000	100	3.0930	90	–	–
2.869–2.888	2.8700	75	2.8780	50	–	–
2.818–2.828	–	–	2.8170	85	2.8143	57
2.607–2.613	2.5600	70	–	–	2.6033	44
2.478–2.485	–	–	–	–	2.4759	100
2.27–2.271	2.2800	40	–	–	–	–

overlapped by those of γ-$Zn_3(VO_4)_2$ and ZnO. The peaks at ~3.20 and ~2.88 Å imply that there is γ-$Zn_3(VO_4)_2$ existing in the samples. Furthermore, a sole peak at ~2.27 Å found in the XRD patterns is exactly corresponding to the peak of phase γ-$Zn_3(VO_4)_2$, which reveals the existence of phase γ-$Zn_3(VO_4)_2$ in all the samples sintered at 900 °C. The SEM EDS (energy dispersive spectra via SEM) analyses on the surface of the ZnO–6 wt.% ($PbO + B_2O_3$)–0.5 mol% V_2O_5–1 mol% MnO_2 ceramics sintered at 950 °C for 2 h show that lead and vanadium are mainly located at the boundaries of ZnO grains, as shown in Fig. 2. These results further indicate that the second phase is zinc lead vanadate. On the other hand, the phase diagrams[34] among ZnO, PbO, B_2O_3 and V_2O_5 show that B_2O_3–V_2O_5 binary system is a kind of completely miscible system and many kinds of compounds are easy to form among them. Thus, it could be suggested that the second phase is a kind of phase γ-$Zn_3(VO_4)_2$ dissolved Pb and B even though no evidence shows that there exists B at the boundaries between the ZnO grains. The XRD patterns show that ZnB_4O_7 is formed in this ceramic system on condition that the co-doped contents of ($PbO + B_2O_3$) are at 12 wt.%.

It is well-known that γ-$Zn_3(VO_4)_2$ is a kind of non-quenchable high temperature phase,[24,25] and this phase is also detected in the ZnO–V_2O_5 varistors doped with Mn_3O_4, CoO, NiO and Na-glass,[14] this phenomenon is considered to be the stabilized effect of these additives to the high-temperature phase.[24] Simultaneously, the addition of PbO and MnO_2 should make a main contribution to the stabilization of γ-$Zn_3(VO_4)_2$ phase in this study.

On the other hand, many reactions among ZnO, PbO, B_2O_3 and V_2O_5 occur during the sintering process because PbO and B_2O_3 are directly co-doped into the ceramics instead of lead zinc borate frit, and, the productions of such reactions possess high activity. Furthermore, it is drawn out from the phase diagrams that liquid-phase appears at relatively low temperature, such as 300 °C,[34] these obviously promote the sintering properties of this ceramic system and its densification. As shown in Fig. 3, the radial shrinkage ratios of the sintered samples calculated by the formula (2) indicate that the values of the radial shrinkage ratio rise with the increases in sintering temperature and the co-doped amount of PbO and B_2O_3, and the maximum values are obtained when the sintered temperature is at about 800 °C.

Fig. 4a–f show the SEM images of the samples sintered at different temperature and different soaking time. It can be found that the grain sizes of ZnO increase with an increase of the sintering temperature and a prolongation of the soaking time, and, it is also concluded that the co-doped

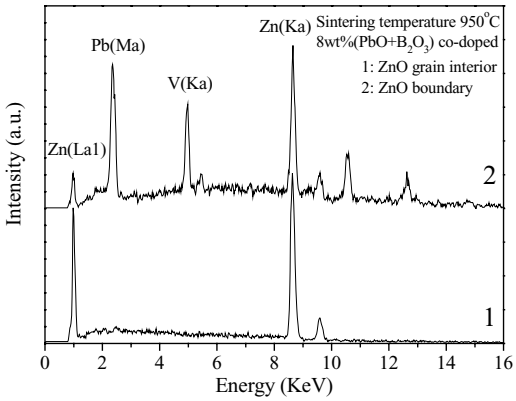

Fig. 2. SEM EDS patterns of the surface of the ZnO–8 wt.% ($PbO+B_2O_3$)–0.5 mol% V_2O_5–1 mol% MnO_2 ceramics sintered at 950 °C for 2 h (curve 1: ZnO grain interior; curve 2: ZnO grain boundary).

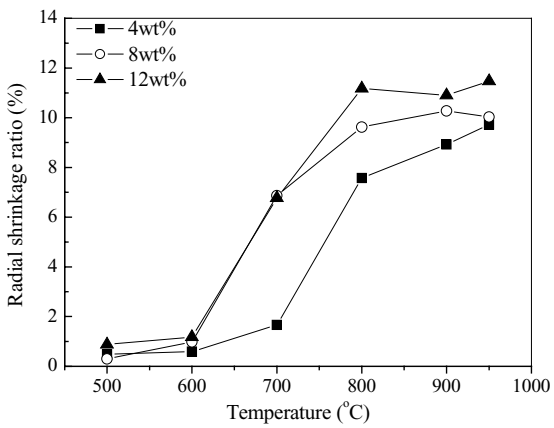

Fig. 3. Dependence of radial shrinkage ratio of the sintered ceramics on the sintering temperature and co-doped amount of PbO and B_2O_3.

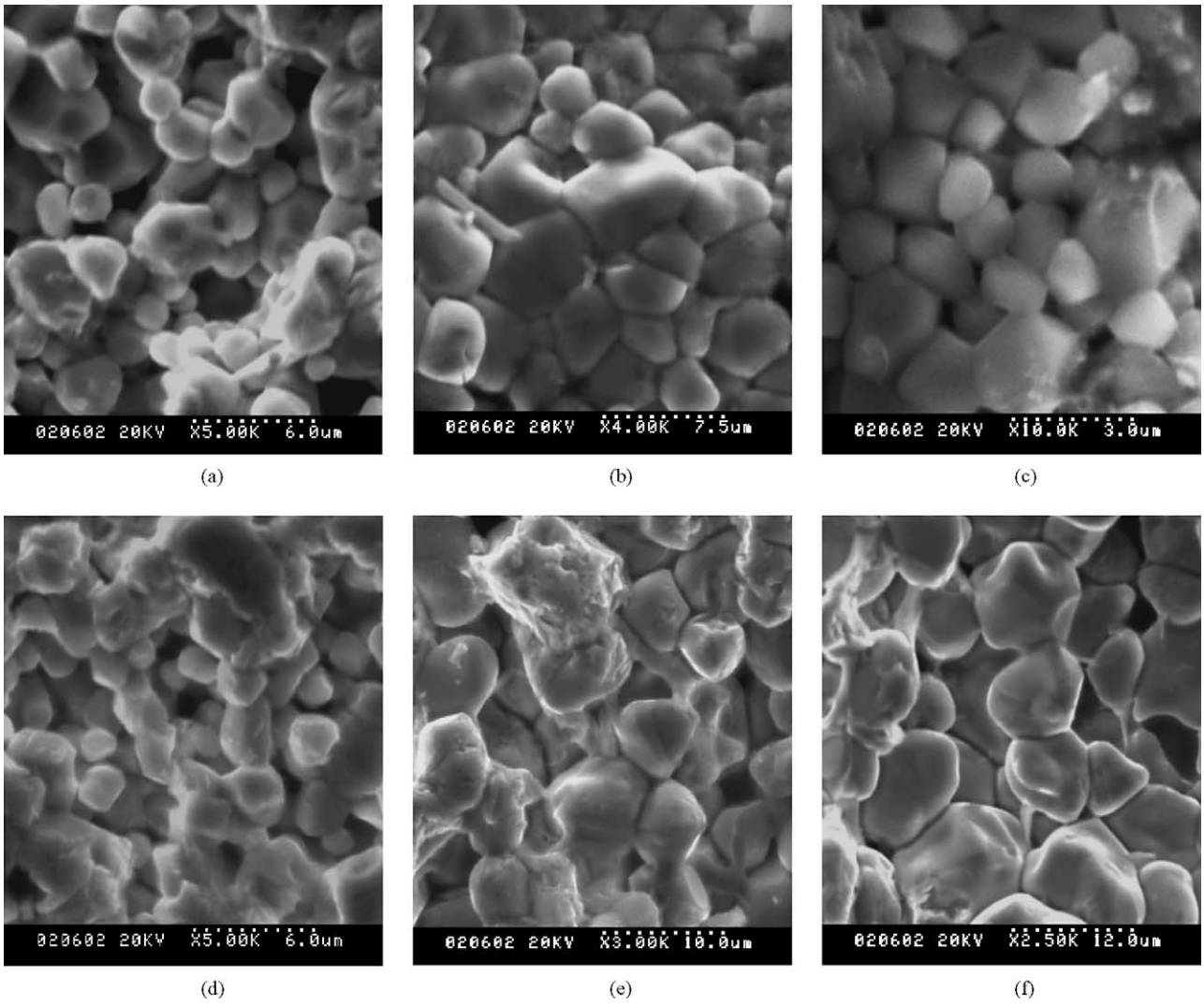

Fig. 4. SEM images of the samples (a) 4 wt.% ($PbO + B_2O_3$) co-doped, sintered at 800 °C for 4 h. (b) 8 wt.% ($PbO + B_2O_3$) co-doped, sintered at 800 °C for 4 h. (c) 12 wt.% ($PbO + B_2O_3$) co-doped, sintered at 800 °C for 4 h. (d) 8 wt.% ($PbO + B_2O_3$) co-doped, sintered at 800 °C for 2 h. (e) 8 wt.% ($PbO + B_2O_3$) co-doped, sintered at 900 °C for 2 h. (f) 8 wt.% ($PbO + B_2O_3$) co-doped, sintered at 950 °C for 2 h.

amount of PbO and B_2O_3 does not significantly influence the phase constituents and morphologies of the sintered ceramics from the SEM images. Simultaneously, the above results also obey a general discipline that sintering temperature and soaking time increase the densification of ceramic materials and enhance the ZnO grain growth rate. As described above, doping PbO and B_2O_3 together causes the liquid-phase sintering and growth of ZnO grains happens at a relatively low temperature just higher above 300 °C drawn out from the phase diagrams,[34] meanwhile, the high activity of the tetrapod ZnO nanopowders further accelerate the growth rate of ZnO grains.

The electrical properties of the samples are characterized by their applied electric field–current density (*E–J*) properties at the pre-breakdown range, as shown in Figs. 5–7. The leakage current density J_L, breakdown field V_{BK} and nonlinear coefficient α are also listed in Table 2. It is evident that the sintering temperature and soaking time markedly

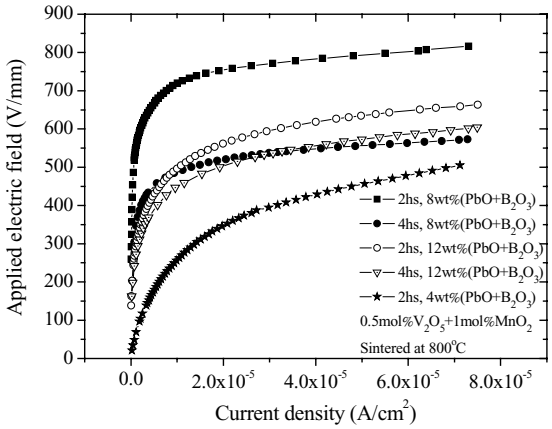

Fig. 5. Effect of the soaking time and co-doped amount of PbO and B_2O_3 on the applied electric field–current density (*E–J*) characteristics of the ZnO–0.5 mol% V_2O_5–1 mol% MnO_2 ceramics sintered at 800 °C.

Table 2
Summary of breakdown field V_{BK}, leakage current density J_L and nonlinear coefficient α of the samples

Specimen number	Content of co-doped ($PbO + B_2O_3$)	Sintering temperature (°C)	Soaking time (h)	Relative density	V_{BK} ($V_{1\,mA}$/mm)	J_L (10^{-6} A/cm^2)	α
A1	8	800	2	0.778	843.8	7.2	21.4
B1	4	800	2	0.671	561.7	–	4.9
C1	12	800	2	0.916	715	24.9	14.8
A2	8	900	2	0.904	389	6.4	21.9
B2	4	900	2	0.808	301	–	4.3
C2	12	900	2	0.980	509	13.7	15.8
A3	8	950	2	0.902	331	6.2	22.8
B3	4	950	2	0.881	213	–	2.05
C3	12	950	2	0.996	290	29.5	16.3
A4	8	800	4	0.755	607	7.2	22.5
B4	4	800	4	0.680	–	–	–
C4	12	800	4	0.921	716	35.6	12.3

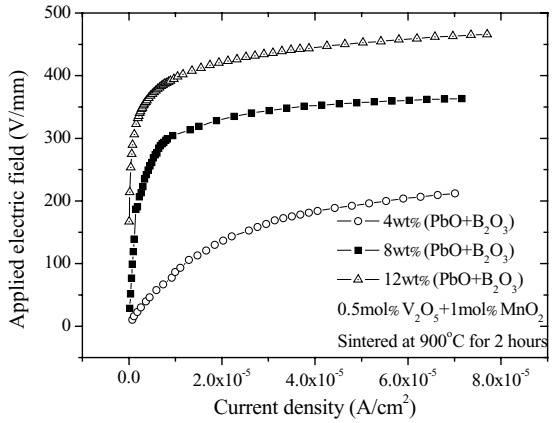

Fig. 6. Effect of the co-doped amount of PbO and B_2O_3 on the applied electric field–current density (E–J) characteristics of the ZnO–0.5 mol% V_2O_5–1 mol% MnO_2 ceramics sintered at 900 °C.

influence the leakage current density J_L, breakdown field V_{BK} and nonlinear coefficient α of the samples with different co-doped contents of PbO and B_2O_3. The breakdown field V_{BK} monotonically decreases with a increasing of the

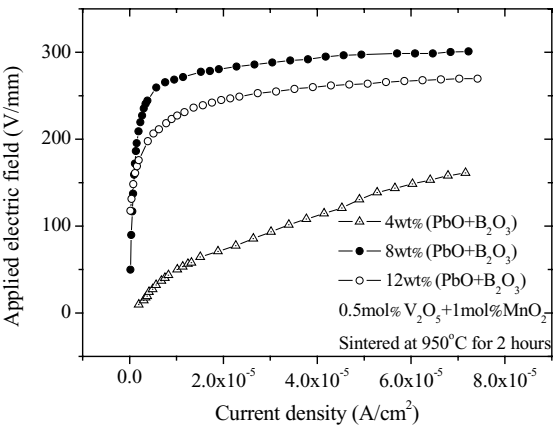

Fig. 7. Effect of the co-doped amount of PbO and B_2O_3 on the applied electric field–current density (E–J) characteristics of the ZnO–0.5 mol% V_2O_5–1 mol% MnO_2 ceramics sintered at 950 °C.

sintering temperature and prolongation of the soaking time. It is worth noticing that the sintering temperature at a range of 800–950 °C has few influence on the leakage current density J_L and nonlinear coefficient α for the samples co-doped with 8 wt.% ($PbO + B_2O_3$). The co-doped amount of PbO and B_2O_3 additives significantly influence the electrical properties of the ZnO–V_2O_5 ceramics. Among all the samples concerning present study, the ZnO–0.5 mol% V_2O_5–1 mol% MnO_2–8 wt.% ($PbO + B_2O_3$) ceramics possesses the following optimum electrical properties: leakage current density $J_L = 6.2 \times 10^{-6}$ A/cm^2, nonlinear coefficient $\alpha = 22.8$ for those sintered at 950 °C for 2 h, and leakage current density $J_L = 7.2 \times 10^{-6}$ A/cm^2, nonlinear coefficient $\alpha = 22.5$ for those sintered at 800 °C for 4 h, respectively. These results indicate that the optimum contents are ZnO–0.5 mol% V_2O_5–1 mol% MnO_2–8 wt.% ($PbO + B_2O_3$) in present work and it is worth noticing that the optimum sintering temperature is closely matching the melting point of Ag conductive paste, (e.g. 960 °C).

It is well known that the nonlinear current–voltage properties of ZnO varistors are mainly contributed by the grain-boundary regions and can be explained by the double Schottky barriers model.[35] For the ZnO–V_2O_5 system, the nonlinear current–voltage behavior can also benefit from the grain-boundary phase γ-$Zn_3(VO_4)_2$. Hng et al. point out that γ-$Zn_3(VO_4)_2$ in the ZnO ceramics doped with V_2O_5 may be a good indicator of desirable varistor behavior.[24] High nonlinear coefficients are obtained for the multicomponent ZnO varistors doped with V_2O_5 and a little amount of Mn_3O_4, CoO, NiO, Nb_2O_5 and Na-glass,[14] and Mn_3O_4 markedly alters the nonohmic behavior of the ZnO–V_2O_5 ceramics.[23] Simultaneously, for the ZnO–B_2O_3–PbO–V_2O_5–MnO_2 ceramics, the nonlinear coefficient can be promoted through co-doping MnO_2, PbO and B_2O_3, because these dopants dissolve in the grain-boundary phase γ-$Zn_3(VO_4)_2$ and stabilize this non-quenchable high temperature phase. Moreover, the function of the doping PbO is similar to that of Bi_2O_3 since Pb^{2-} is a kind of large ions, the residing of Pb^{2-} in the grain-boundary region and the acting as electron traps induce large potential barriers,

increase the nonlinear coefficient and decrease the leakage current density of the materials. PbO and B_2O_3 are the starting materials that prepare lead zinc borate frit which is a kind of varistor formers,[15–20] co-doping of PbO and B_2O_3 can further increase the nonlinear coefficient and decrease the leakage current of the ZnO–V_2O_5 varistors.

4. Conclusion

A peculiar kind of ZnO–B_2O_3–PbO–V_2O_5–MnO_2 varistors is produced by sintering in conventional electric furnace operated at a low temperature of 800 °C. The readily-achieved process benefits from the addition of B_2O_3 and V_2O_5, which promote diffusion in the doped ZnO materials, especially when ZnO starting materials are ZnO nanopowders. PbO and MnO_2 help to stabilize the high-temperature phase γ-$Zn_3(VO_4)_2$. The co-doping of PbO and B_2O_3 significantly enhances electrical properties of the ZnO–V_2O_5 varistors. When the ceramics are co-doped with 8 wt.% (PbO+B_2O_3) and sintered at 950 °C for 2 h, the optimum electrical properties of $J_L = 6.2 \times 10^{-6}$ A/cm^2, $\alpha = 22.8$ and $V_{BK} = 331$ V/mm are obtained. The sintering temperature has almost no evidently influence on the nonlinear coefficient α and leakage current density J_L of the ZnO–0.5 mol% V_2O_5–1 mol% MnO_2–8 wt.% (PbO+B_2O_3) ceramics at the range of 800–950 °C. The produced ceramics display a potential application in multilayer varistors.

Acknowledgements

This work is supported by the Key Project for Science and Technology Research of Ministry of Education (Grant No. 00084), Science and Technology Planning Project of Wuhan (Grant No. 20011007088-5).

The authors gratefully thank Professor Liu Xinglang for her some valuable suggestions to this paper.

References

1. Matsuoka, M., Masuyama, T. and Iida, Y., Voltage nonlinearity of zinc oxide ceramics doped with alkali-earth metal oxide. *Jpn. J. Appl. Phys.* 1969, **8**, 1275–1276.
2. Matsuoka, M., Non-ohmic properties of zinc oxide ceramics. *Jpn. J. Appl. Phys.* 1971, **10**, 736–746.
3. Masanori, I., Crystal phases of nonohmic zinc oxide ceramics. *Jpn. J. Appl. Phys.* 1978, **17**, 1–10.
4. Kazuo, E., Atsushi, I. and Matsuoka, M., Degradation mechanism of non-ohmic zinc oxide ceramics. *J. Appl. Phys.* 1980, **51**, 2678–2684.
5. Levinson, L. M. and Philipp, H. R., Zinc oxide varistors—a review. *Am. Ceram. Soc. Bull.* 1986, **65**, 639–646.
6. Gupta, T. K., Applications of zinc oxide varistors. *J. Am. Ceram. Soc.* 1990, **73**, 1817–1840.
7. Wong, J., Sintering and varistor characteristics of ZnO–Bi_2O_3 ceramics. *J. Appl. Phys.* 1980, **51**, 4453–4459.
8. Alles, A. B. and Burdick, V. L., The effect of liquid-phase sintering on the properties of Pr_6O_{11}-based ZnO varistors. *J. Appl. Phys.* 1991, **70**, 6883–6890.
9. Alles, A. B., Puskas, R., Callahan, G. and Burdick, V. L., Compositional effects on the liquid-phase sintering of praseodymium oxide-based zinc oxide varistors. *J. Am. Ceram. Soc.* 1993, **76**, 2098–2102.
10. Caballero, A. C., Valle, F. J., Villegas, M., Moure, C., Duraân, P. and Fernândez, J.F., Improved chemical stability of ZnO–BaO based varistors. *J. Eur. Ceram. Soc.* 2000, **20**, 2767–2772.
11. Tsai, J. K. and Wu, T. B., Non-ohmic characteristics of ZnO–V_2O_5 ceramics. *J. Appl. Phys.* 1994, **76**, 4817–4822.
12. Tsai, J.-K. and Wu, T.-B., Microstructure and non-ohmic properties of ZnO–V_2O_5 ceramics. *Jpn. J. Appl. Phys.* 1995, **34**, 6452–6457.
13. Tsai, J.-K. and Wu, T.-B., Microstructure and nonohmic properties of binary ZnO–V_2O_5 ceramics sintered at 900 °C. *Mater. Lett.* 1996, **26**, 199–203.
14. Chen, C.-S., Kuo, C.-T., Wu, T.-B. and Lin, I.-N., Microstructure and electrical properties of V_2O_5-based multicomponent ZnO varistors prepared by microwave sintering process. *Jpn. J. Appl. Phys.* 1997, **36**, 1169–1175.
15. Shohata, N. and Yoshida, J., Effect of glass on non-ohmic properties of ZnO ceramics varistors. *Jpn. J. Appl. Phys.* 1977, **16**, 2299–2300.
16. Lee, Y.-S. and Tseng, T.-Y., Phase identification and electrical properties in ZnO-glass varistors. *J. Am. Ceram. Soc.* 1992, **75**, 1636–1640.
17. Lin, J. N., Lin, C. M., Kao, C. C. and Chang, W. C., Electrical properties and degradation phonemena of glass-doped ZnO chip varistors. *Mater. Sci. Eng. B* 1993, **20**, 261–265.
18. Yen, A.-J., Lee, Y.-S. and Tseng, T.-Y., Electrical properties of multilayer-chip ZnO varistors in a moist-air environment. *J. Am. Ceram. Soc.* 1994, **77**, 3006–3011.
19. Lee, Y.-S. and Tseng, T.-Y., Influence of processing parameters on the microstructure and electrical properties of multilayer-chip ZnO varistors. *J. Mater. Sci., Mater. Electron.* 1995, **6**, 90–96.
20. Lee, Y.-S. and Tseng, T.-Y., Correlation of grain boundary characteristics with electrical properties in ZnO-glass varistors. *J. Mater. Sci., Mater. Electron.* 1998, **9**, 65–76.
21. Kurzawa, M., Rychlowska-Himmel, I., Bosacka, M. and Blonska-Tabero, A., Reinvestigation of phase equilibria in the V_2O_5–ZnO system. *J. Them. Anal. Cal.* 2001, **64**, 1113–1119.
22. Kuo, C.-T., Chen, C.-S. and Lin, I.-N., Microstructure and nonlinear properties of microwave-sintered ZnO–V_2O_5 varistors. I. Effect of V_2O_5 doping. *J. Am. Ceram. Soc.* 1998, **81**, 2942–2948.
23. Kuo, C.-T., Chen, C.-S. and Lin, I.-N., Microstructure and nonlinear properties of microwave-sintered ZnO–V_2O_5 varistors. II. Effect of Mn_3O_4 doping. *J. Am. Ceram. Soc.* 1998, **81**, 2949–2956.
24. Hng, H.-H. and Knowles, K. M., Characterisation of $Zn_2(VO_4)_2$ phases in V_2O_5-doped ZnO varistors. *J. Eur. Ceram. Soc.* 1999, **9**, 721–726.
25. Hng, H.-H. and Knowles, K. M., Microstructure and current–voltage characteristics of multicomponent vanadium-doped zinc oxide varistors. *J. Am. Ceram. Soc.* 2000, **83**, 2455–2462.
26. Shioziri, M. and Kaito, C., Structure and growth of ZnO smoke particles prepared by gas evaporation technique. *J. Cryst. Growth* 1981, **52**, 173–177.
27. Suyama, Y., Tomokiyo, Y., Manabe, T. and Tanaka, E., Shape and structure of zinc oxide particles prepared by vapor-phase oxidation of zinc vapor. *J. Am. Ceram. Soc.* 1988, **71**, 391–395.
28. Run, W., Changsheng, X., Hui, X., Junhui, H. and Aihua, W., The thermal physical formation of ZnO nanoparticles and their morphology. *J. Cryst. Growth* 2000, **217**, 274–280.
29. Ya, K. X., Yin, H., De, T. M. and Jing, T. M., Analysis of ZnO varistors prepared from nanosize ZnO precursors. *Mater. Res. Bull.* 1998, **33**, 1703–1708.

30. Lin, Y., Zhang, Z., Tang, Z., Yuan, F. and Li, J., Characterization of ZnO-based varistors prepared from nanometre precursor powders. *Adv. Mater. Opt. Electron.* 1999, **9**, 205–209.
31. Kong, L., Li, F., Zhang, L. and Yao, X., Sol–gel glass-coated zinc oxide for varistor applications. *J. Mater. Sci. Lett.* 1998, **17**, 769–771.
32. Durán, P., Capel, F., Tartaj, J. and Moure, C., Sintering behavior and electrical properties of nanosized doped-ZnO powders produced by metallorganic polymeric processing. *J. Am. Cream. Soc.* 2001, **84**, 1661–1668.
33. Jun, W., Changsheng, X., Zikui, B., Bailin, Z., Kaijin, H. and Run, W., Preparation of ZnO-glass varistor from tetrapod ZnO nanopowders. *Mater. Sci. Eng. B* 2002, **95**, 157–161.
34. Roth, R. S., Clevinger, M. A., McKenna, D. and Smith, G., *Phase Diagrams for Ceramists*. American Ceramic Society, Columbus, OH, 1984, pp. 98, 115, 117, 119, 222.
35. Clarke, D. R., Varistors ceramics. *J. Am. Ceram. Soc.* 1999, **82**, 485–502.